

Two-dimensional CrP_2 with high specific capacity and fast charge rate for lithium-ion battery

Xiaoyun Wang(王晓允), Tao Jing(荆涛), and Dongmei Liang(梁冬梅)
Citation: Chin. Phys. B, 2023, 32 (**6**): 067102. DOI: 10.1088/1674-1056/acc5e0
Journal homepage: http://cpb.iphy.ac.cn; http://iopscience.iop.org/cpb

What follows is a list of articles you may be interested in

Predicting novel atomic structure of the lowest-energy Fe_nP_{13-n} (n=0-13) clusters: A new parameter for characterizing chemical stability

Yuanqi Jiang(蒋元祺) and Ping Peng(彭平)
Chin. Phys. B, 2023, 32 (**4**): 047102. DOI: 10.1088/1674-1056/acae75

High-temperature ferromagnetism and strong π-conjugation feature in two-dimensional manganese tetranitride

Ming Yan(闫明), Zhi-Yuan Xie(谢志远), and Miao Gao(高淼)
Chin. Phys. B, 2023, 32 (**3**): 037104. DOI: 10.1088/1674-1056/acae7b

Site selective 5f electronic correlations in β-uranium

Ruizhi Qiu(邱睿智), Liuhua Xie(谢刘桦), and Li Huang(黄理)
Chin. Phys. B, 2023, 32 (**1**): 017101. DOI: 10.1088/1674-1056/ac76ad

Modulation of Schottky barrier in XSi_2N_4/graphene (X=Mo and W) heterojunctions by biaxial strain

Qian Liang(梁前), Xiang-Yan Luo(罗祥燕), Yi-Xin Wang(王熠欣), Yong-Chao Liang(梁永超), and Quan Xie(谢泉)
Chin. Phys. B, 2022, 31 (**8**): 087101. DOI: 10.1088/1674-1056/ac5c3b

Interfacial defect engineering and photocatalysis properties of hBN/MX_2 (M = Mo, W, and X = S, Se heterostructures

Zhi-Hai Sun(孙志海), Jia-Xi Liu(刘佳溪), Ying Zhang(张颖), Zi-Yuan Li(李子源), Le-Yu Peng(彭乐宇), Peng-Ru Huang(黄鹏儒), Yong-Jin Zou(邹勇进), Fen Xu(徐芬), and Li-Xian Sun(孙立贤)
Chin. Phys. B, 2022, 31 (**6**): 067101. DOI: 10.1088/1674-1056/ac43b2

Two-dimensional CrP_2 with high specific capacity and fast charge rate for lithium-ion battery

Xiaoyun Wang(王晓允)[1], Tao Jing(荆涛)[2,†], and Dongmei Liang(梁冬梅)[2]

[1] *College of Electrical and Mechanical Engineering, Xuchang University, Xuchang* 461000, *China*
[2] *College of Science, Kaili University, Kaili* 556011, *China*

(Received 9 January 2023; revised manuscript received 19 March 2023; accepted manuscript online 21 March 2023)

The electrode material is regarded as one of the key factors that determine the performance of lithium-ion batteries (LIBs). However, it is still a challenge to search for an anode material with large capacity, low diffusion barrier, and good stability. In the present work, two new CrP_2 monolayers (*Pmmn*-CrP_2 and *Pmma*-CrP_2) are predicted by means of first principles swarm structure search. Our study shows that both the two CrP_2 monolayers have high dynamical and thermal stability, as well as excellent electron conductivity. Additionally, *Pmmn*-CrP_2 exhibits a remarkably high storage capacity of 705 mA·h·g^{-1} for Li, meanwhile the diffusion energy barrier of Li on the surface of this monolayer is 0.21 eV, ensuring it as a high-performance anode material for LIBs. We hope that our study will inspire researchers to search for new-type two-dimensional (2D) transition metal phosphides for the electrode materials of LIBs.

Keywords: lithium-ion battery, electronic structure, first principles

PACS: 71.20.–b

DOI: 10.1088/1674-1056/acc5e0

1. Introduction

As a mature technology for electrical energy storage, rechargeable lithium-ion batteries (LIBs) have been widely used in portable electronic and electric vehicles.[1–3] Nevertheless, with the increased demands for large-scale energy storage equipment, the current commercial LIBs are still far from satisfactory.[4–6] It has been widely accepted that the constituent electrode is one of the key factors to determine the performance of LIBs.[7,8] Currently, graphite is used as the most common anode material for LIBs, partly owning to its low cost and good cycling stability. However, the relatively low specific capacity and poor rate capacity of graphite electrode are the main bottlenecks to restrict its performance.[9–11] To date, numerous studies have focused on the improved performance of electrode for LIBs. For example, a unique micro-sized silicon composite anode has been synthesized, exhibiting significantly enhanced Li-ion battery performances.[12] Recently, it has been shown that Fermi level tuning by p-type doping can be an effective way of dramatically raising electrode potential.[13] However, the searching of new anode materials with large capacity, low diffusion barrier, and good stability is still important for realizing the large-scale utilization of LIBs.[14,15]

Two-dimensional (2D) materials with many fascinating properties including the remarkably high carrier mobility, outstanding mechanical flexibility, and large surface-to-volume ratio, have great potential in technological applications.[16] Recently, many 2D materials have been proposed theoretically as a promising candidate for applications in LIBs.[17–19] Multiscale computation methods, including first-principles calculation, molecular dynamics simulation, phase field simulation, finite element, and machine learning, can be applied in discovery and design of new electrode materials.[12] As a relatively new family of monolayer materials, 2D transition metal carbides and nitrides with a general formula of $M_{n+1}X_n$, namely MXenes, show promising applications as anode materials for LIBs, in view of their excellent electron conduction and high charge/discharge rates.[20,21] For example, Ti_2C was synthesized experimentally as an anode material for LIBs and it displayed a specific capacity of 225 mA·h·g^{-1}.[22] Mo_2C monolayer was predicted theoretically to possess a high theoretical capacity of 526 mA·h·g^{-1} and a minimal diffusion barrier of 0.035 eV only.[23] However, MXenes were known to have less chemically stable and low specific capacity for Li. The reason can be attributed to the direct exposure of metal atoms on the surfaces of MXenes, greatly weakening the adsorption strength between Li and the support.[24] In addition, several kinds of functional groups including OH, O, and F are introduced on the surfaces of MXenes in the process of experimental synthesis, which can reduce specific capacity and increase the diffusion energy barrier for Li simultaneously.[25–27] Therefore, the increase of carbon or nitrogen composition in MXenes provides a direct and effective strategy to promote their performance as anode materials for LIBs. To date, several carbon or nitrogen-rich monolayers, such as MoC, MoN, TaC_2, VC_2, ScN_2, VN_2, TiC_3, and NiC_3, have been theoretical proposed and exhibited remarkably improved specific capacity for Li.[28–34]

As a promising candidate to replace graphite electrode, black phosphorus possesses a wide application prospect in

†Corresponding author. E-mail: jingt87@sina.com

© 2023 Chinese Physical Society and IOP Publishing Ltd

LIBs due to its abundant resource and outstanding specific theoretical capacity of 2596 mA·h·g^{-1}.[35] However, the occurrence of huge volume expansion of about 400% leads to the rapid capacity loss and safety issues during the charge/discharge process.[36] Recently, it has been predicted that the Li capacity of MXenes, including Ti_2C and V_2C, can be remarkably enhanced by surface functionalization of P atoms, and the value of which is as high as 1767 mA·h·g^{-1}.[37] This striking improvement can be ascribed to the strong adsorption of P for Li. Inspired by this, thus, we explore the potential of 2D transition metal phosphides for anode materials of LIBs. The direct exposure of P on the surfaces of these monolayers is expected to promote the Li adsorption and improve the Li capacity for LIBs.

In the present work, we propose two new CrP_2 monolayers by combining the global minimum structure search with first-principles calculations. We find that CrP_2 monolayers are mechanical, dynamical, and thermal stable. The investigations of electronic structures indicate that the two CrP_2 monolayers possess good electronic conductivity. In addition, the high theoretical capacity and low diffusion barriers render the CrP_2 monolayers as promising anode materials for LIBs. Our work might inspire people to study transition metal phosphides as potential applications for LIBs.

2. Calculation method

The structural predication of CrP_2 monolayers is carried out based on particle swarm optimization (PSO) method, as implemented in CALYPSO code.[38] The population size and the number of generations are set as 40 and 30, respectively, to ensure convergence. The first-principles calculations are performed within the density functional theory (DFT) formalism as implemented in VASP.[39] The electron–ion interactions are included using the frozen-core projected augmented wave (PAW) approach with the cutoff energy of 500 eV.[40] The exchange–correlation energy is described using the generalized gradient approximation (GGA) in the form of Perdew–Bruke–Ernzerhof (PBE).[41] The Monkhorst–Pack k-point meshes of $19\times13\times1$ and $5\times5\times1$ are used for unit cell and supercell calculations, respectively. In the calculations of structural optimization, the convergence tolerance for energy and force are set to be 10^{-6} eV and 0.01 eV/Å. To avoid interaction between adjacent layers, a sufficiently large vacuum thickness of 20 Å is adopted. AIMD simulations are carried out to inspect the thermal stability of these monolayers at 1500 K for 5 ps with a time step of 1 fs. The phonon frequencies are calculated by using a supercell approach as implemented in the PHONOPY code.[42] The climbing image nudged elastic band (CI-NEB) method is employed to estimate the diffusion energy barrier and the minimum energy pathway for Li on CrP_2 monolayers.[43,44]

To quantitatively describe the energetic stability of CrP_2 monolayer, the cohesive energy (E_{coh}) is calculated according to the expression

$$E_{coh}=\frac{E_{CrP_2}-E_{Cr}-2E_P}{3},$$

where E_{CrP_2} and $E_{Cr(P)}$ represent the total energies of CrP_2 monolayer and a single Cr (P) atom, respectively. According to this definition, a more negative value of cohesive energy implies the higher energetic stability of this monolayer.

To evaluate the adsorption strength of Li on the surface of CrP_2 monolayers, a 3×2 supercell is adopted, which is large enough to avoid interaction between adjacent Li atoms. Here, the adsorption energy can be evaluated by the following formula:

$$E_{ad}=E_{M+CrP_2}-E_{CrP_2}-E_M,$$

where E_{M+CrP_2} and E_{CrP_2} are the total energies of the Li-adsorbed and pristine CrP_2 monolayers, respectively, and E_M is the energy of an Li atom in bulk structure.

For multilayer adsorption, the average adsorption energy is calculated layer by layer, as defined by

$$E_{ave}=\frac{E_{4nM+CrP_2}-E_{CrP_2+4(n-1)M}-4E_M}{4}.$$

The theoretical capacity for Li is computed as follows:

$$C_M=\frac{nF}{M_{CrP_2}},$$

where n is the valance number of Li atoms, F represents the Faraday constant (26798 mA·h·mol^{-1}), and M_{CrP_2} is the molar weight of CrP_2.

The open circuit voltage (OCV) can be estimated from the following reaction:

$$CrP_2+nLi^++ne^-\longleftrightarrow Li_nCrP_2,$$

thus, the open-circuit voltage (OCV) is accessed by

$$OCV=\frac{E_{CrP_2}+nE_{Li}-E_{Li_nCrP_2}}{ne}.$$

3. Results and discussion

3.1. Structure and stability of CrP_2 monolayers

All possible 2D planar structures of CrP_2 are searched by the particle swarm optimization (PSO) structure search method. We focus on two most energetically stable CrP_2 monolayers, which both belong to the orthorhombic system, as demonstrated in Fig. 1. The space groups of the two monolayers are *Pmmn* and *Pmma*, which are labeled as *Pmmn*-CrP_2 and *Pmma*-CrP_2, respectively. In the optimized structures, each Cr atom in *Pmmn*-CrP_2 is surrounded by six P atoms, while each P atom is bonded to three Cr atoms and two P atoms, forming a one-dimensional chain structure (P–P–P) along the y direction. In light of the direct exposure of P atoms on the surface, it is rational to predict that *Pmmn*-CrP_2 can be an ideal substrate for the Li adsorption. In the

case of *Pmma*-CrP_2, Cr atoms form zigzag chains along the *x* direction, which are sandwiched between two P atomic layers. These in-plane P–Cr–P layers are connected by P–P bonds along the *y* direction. It is noteworthy that the Cr atoms in *Pmma*-CrP_2 are closer to the surface than those of *Pmmn*-CrP_2, reducing the adsorption strength between Li and the substrate. The lattice parameters of *Pmmn*-CrP_2 are calculated to be $a = 3.13$ Å and $b = 4.68$ Å, while those for *Pmma*-CrP_2 are $a = 3.76$ Å and $b = 4.85$ Å.

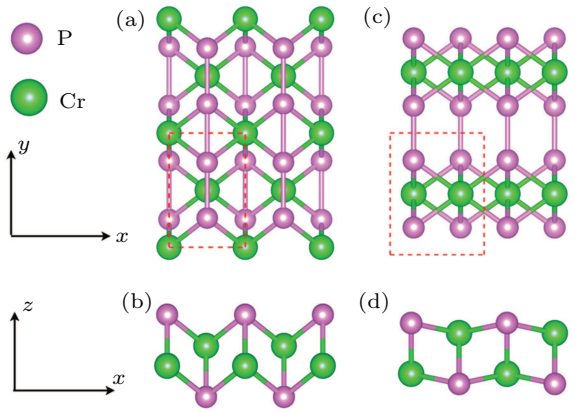


Fig. 1. Top and side views of atomic structures for [(a), (b)] *Pmmn*-CrP_2 and [(c), (d)] *Pmma*-CrP_2.

Cohesive energy is usually employed to access the energetic stability and experimental feasibility of predicted 2D materials. The resultant cohesive energy of *Pmmn*-CrP_2 is −6.92 eV per atom, while that for *Pmma*-CrP_2 is −6.73 eV per atom, both of which are much lower than that of P_3C (4.18 eV per atom),[36] phosphorene (−3.48 eV per atom),[45] SnP_3 (−3.88 eV per atom),[46] and GeP_3 (−3.34 eV per atom),[47] implying their high energetic stability. Next, we examine the dynamical stability of the predicted monolayers, thus the phonon spectra along the high-symmetry lines is calculated using DFPT method, as plotted in Figs. 2(a) and 2(b). The absence of any appreciable imaginary frequency is found in the full Brillouin zone, confirming the dynamical stability of the two CrP_2 monolayers. For an evaluation of the thermal stability of the two CrP_2 monolayers, we perform the AIMD simulations at 1500 K lasted for 5 ps.[48] As depicted in Figs. 2(c) and 2(d), the atomic configurations of the two CrP_2 monolayers are well maintained and no notable distortion is found for the crystal structures, suggesting that the two monolayers can withstand the high temperature of over 1500 K. Besides, it is noted that the total energy fluctuates of the two CrP_2 monolayers are considerably small at 1500 K, further verifying their extremely high thermal stability.

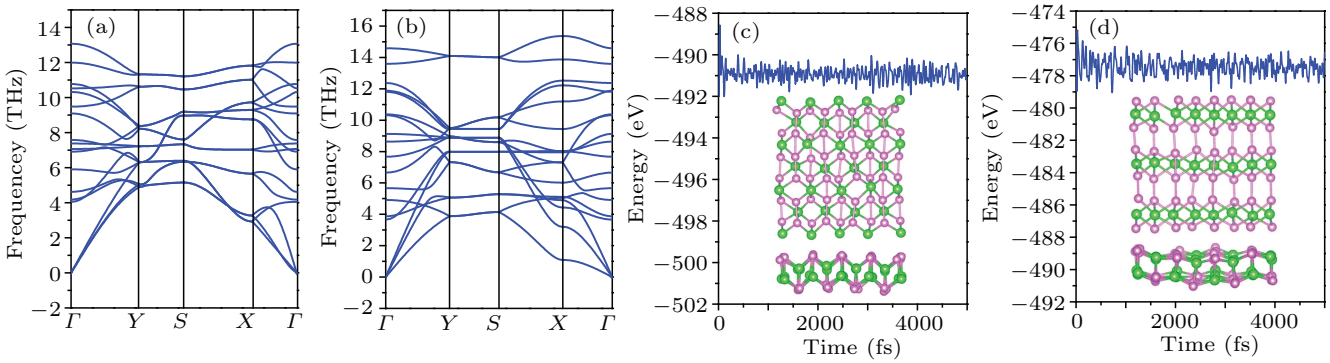


Fig. 2. The phonon dispersion curves of (a) *Pmmn*-CrP_2 and (b) *Pmma*-CrP_2. Total potential energy fluctuations and the corresponding snapshots of (c) *Pmmn*-CrP_2 and (d) *Pmma*-CrP_2 after 5 ps of AIMD simulation at 1500 K.

3.2. Electronic and mechanical properties of CrP_2 monolayers

Then, the band structures and projected density of states (PDOS) of *Pmmn*-CrP_2 and *Pmma*-CrP_2 are investigated, as illustrated in Figs. 3(a) and 3(b). We note that both *Pmmn*-CrP_2 and *Pmma*-CrP_2 show the metallic properties with high DOS peaks crossing the Fermi level. This means that the two monolayers have outstanding electronic conductivity, thereby leading to the fast charge transfer during the charge/discharge process. Further analysis of PDOS reveals that the electronic states near the Fermi level are dominated by the 3d orbitals of Cr atoms, while the 3p orbitals of P atoms make a relatively small contribution to these states. To figure out the bonding features of the two CrP_2 monolayers, we plot electron localization function (ELF), as presented in Figs. 3(c) and 3(d). It is found that P–P bond exhibits strongly covalent bond characteristics, but Cr–P bond is identified as a typical ionic bond. Significantly, the formation of P–P covalent bonds in CrP_2 monolayers can reduce the total energies and increase their structural stability. Bader charge analysis implies that a significant amount of electrons is transferred from each Cr atom to P atoms (0.71*e* for *Pmmn*-CrP_2 and 0.74*e* for *Pmma*-CrP_2).

Now we turn to the mechanical properties of the two CrP_2 monolayers and the elastic constants are firstly calculated. For *Pmmn*-CrP_2 (*Pmma*-CrP_2), C_{11}, C_{22}, C_{12}, and C_{66} are 62.28 N/m, 190.58 N/m, 25.03 N/m, and 37.77 N/m (115.38 N/m, 170.19 N/m, 48.79 N/m, and 47.13 N/m), respectively. It is noted that the value of $C_{11}C_{22}$ is larger than that of the C_{12}^2, meanwhile C_{66} has a positive value, verifying the mechanically stability of the two CrP_2 monolayers. Based on these elastic constants, we also assess the in-plane Young's

moduli (Y) of the CrP_2 monolayers using the following equation:

$$E_x = \frac{(C_{11}C_{22} - C_{12}^2)}{C_{22}}, \quad E_y = \frac{(C_{11}C_{22} - C_{12}^2)}{C_{11}}.$$

The in-plane Young's moduli of *Pmmn*-CrP_2 (*Pmma*-CrP_2) are 58.99 (101.39) N/m and 180.52 (149.55) N/m in the *x* and *y* directions, respectively. We note that the in-plane Young's moduli of the two monolayers are less than those of hexagonal h-BN (271 N/m)[49] and graphene (340 N/m),[50] indicative of their good mechanical flexibility.

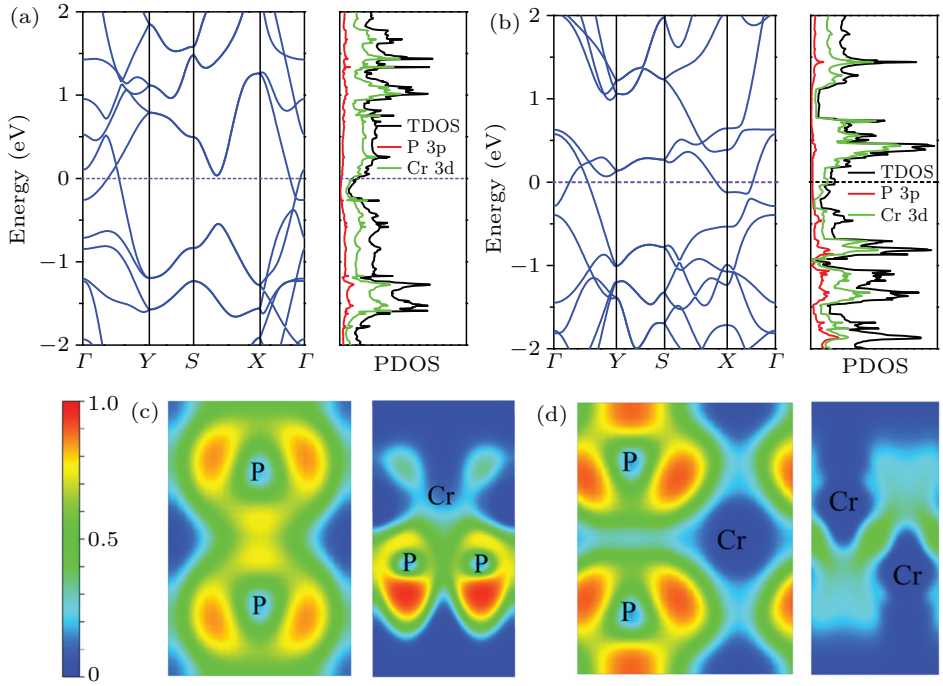


Fig. 3. The calculate band structure and partial density of states (PDOS) of (a) *Pmmn*-CrP_2 and (b) *Pmma*-CrP_2. Electron localization function (ELF) map of (c) *Pmmn*-CrP_2 and (d) *Pmma*-CrP_2.

3.3. Adsorption and diffusion behaviors of Li on CrP_2 monolayers

To explore the adsorption and diffusion behaviors of Li on the surfaces of CrP_2 monolayer, the most stable adsorption site should be determined firstly. Considering the lattice symmetry, four representative adsorption sites are chosen for each CrP_2 monolayer to explore the Li adsorption properties on the substrate, as shown in Figs. 4(a) and 4(b). Notably, a negative value of adsorption energy corresponds to an exothermic reaction. For *Pmmn*-CrP_2 (*Pmma*-CrP_2), A_1 and A_4 (B_2 and B_4) locate just above the top and bottom Cr atoms, respectively, while A_3 and A_2 (B_3 and B_1) are above the center of top and bottom P–P bonds. For various sites, the calculated adsorption energies of Li are summered in Table 1. In the case of *Pmmn*-CrP_2, the adsorption energies of Li on A_1, A_2, A_3, and A_4 sites are −1.19 eV, −1.08 eV, −0.76 eV, and −0.83 eV, respectively, showing the strong interaction between Li and the support. We also note that Li atom prefers to be absorbed at the A_1 site of *Pmmn*-CrP_2 due to the lowest adsorption energy. For *Pmma*-CrP_2, the adsorption energies of Li on B_1, B_2, B_3, and B_4 sites are predicted to be −1.41 eV, −0.94 eV, −0.77 eV, and −1.08 eV, correspondingly. Obviously, B_1 is the optimal position for Li adsorption and much more stable than other sites.

Table 1. The Li adsorption energies on high-symmetry sites for *Pmmn*-CrP_2 and *Pmma*-CrP_2 monolayers.

Pmmn-CrP_2				
	A_1	A_2	A_3	A_4
E_{ad} (eV)	–1.19	–1.08	–0.76	–0.83
Pmma-CrP_2				
	B_1	B_2	B_3	B_4
E_{ad} (eV)	–1.41	–0.94	–0.77	–1.08

Since the number of adsorbed Li atoms directly correlates with the theoretical capacity of the anode materials for LIBs, thus we explore the concentration-dependent Li adsorption behavior by applying a $3 \times 2 \times 1$ CrP_2 supercell. Notably, once the value of adsorption energy becomes positive, the Li atoms on the surface of CrP_2 monolayer are inclined to agglomerate. We consider the adsorption of Li on both sides of the slab and calculate the average adsorption energy for each Li layer. Structurally, Li atoms are placed successively on the sites A_1, A_2, A_4, and A_1 for the first, second, third, and fourth layers, respectively, until all possible sites are occupied. Very interesting, the average adsorption energy of Li on *Pmmn*-CrP_2 is still negative when the number of adsorbed Li layers reaches three, corresponding to the stoichiometry of Li_3CrP_2. In addition, the average adsorption energies decrease steadily with the increasing the number of Li layers. Thus,

the theoretical specific capacity of Li on *Pmmn*-CrP_2 reaches as high as 705 mA·h·g^{-1}, which is significantly larger than that of graphite (372 mA·h·g^{-1}).[51] As presented in Fig. 4(b), *Pmma*-CrP_2 can adsorb only two layer of Li, corresponding to the stoichiometry of Li_2CrP_2. The theoretical specific capacity of this monolayer is estimated to be 470 mA·h·g^{-1}. Compared with *Pmmn*-CrP_2, the lower value of specific capacity can be ascribed to the direct exposure of Cr atoms on the surface of *Pmma*-CrP_2, which enhances the repulsion interactions between Li and the support.

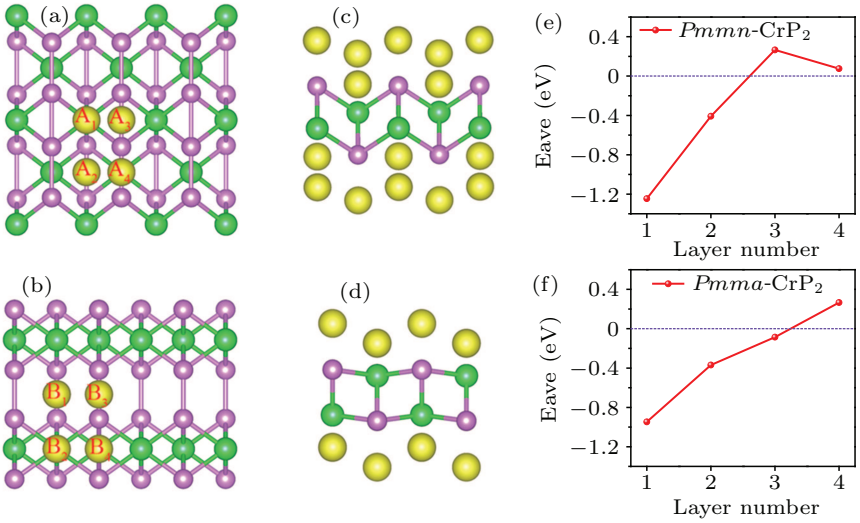


Fig. 4. The Li adsorption sites for (a) *Pmmn*-CrP_2 and (d) *Pmma*-CrP_2. Atomic structures of (c) *Pmmn*-CrP_2 with three-layer Li adsorption and (d) *Pmma*-CrP_2 with two-layer Li adsorption. Adsorption energies with the increase of Li concentration for (e) *Pmmn*-CrP_2 and (f) *Pmma*-CrP_2.

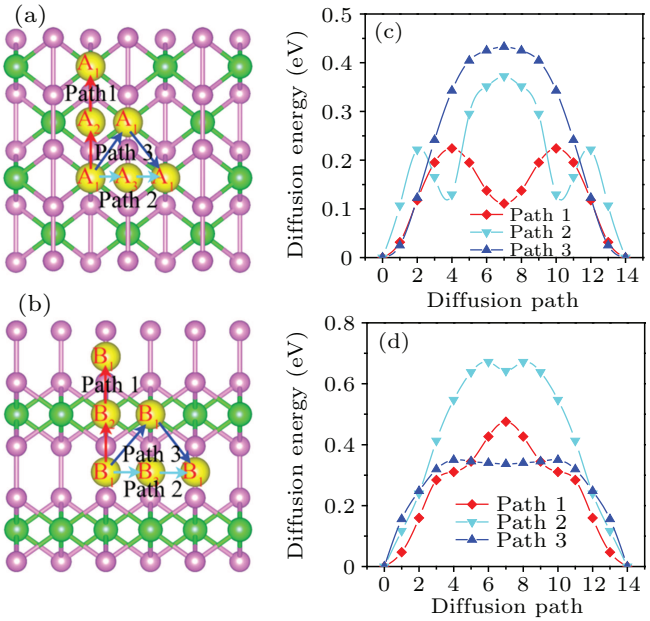


Fig. 5. The considered diffusion paths of Li on (a) *Pmmn*-CrP_2 and (b) *Pmma*-CrP_2. The diffusion energy barrier profiles of Li on (c) *Pmmn*-CrP_2 and (d) *Pmma*-CrP_2.

The diffusion behavior of Li on the surface of anode materials was shown to be crucial for the performance of charging/discharging process and circulation efficiency in LIBs.[52,53] Therefore, the diffusion pathways and the corresponding diffusion barriers of Li on the $3 \times 2 \times 1$ CrP_2 supercell are investigated by the climbing-image nudge elastic band (CI-NEB) method. Considering the structural symmetry of *Pmmn*-CrP_2, three possible diffusion pathways are selected for this monolayer, which are marked as path 1, path 2, and path 3, as shown in Fig. 5(a). It is worth noting that the path 1 and path 3 correspond to the Li diffusion on the substrate in the x and y directions, respectively. But along the path 2, Li can diffuse either in the x or y direction. As presented in Fig. 5(b), the corresponding diffusion energy barriers of Li along the path 1, path 2, and path 3 are estimated to be 0.21 eV, 0.36 eV, and 0.43 eV, respectively, revealing that Li prefers to diffuse along the path 1. The low diffusion energy barrier suggests that Li is easily to diffuse on the surface of *Pmmn*-CrP_2, leading to the fast charging/discharging process. In light of *Pmma*-CrP_2, three possible pathways are considered for Li ion diffusion, similar to the case of *Pmmn*-CrP_2. The calculated diffusion energy barriers for path 1, path 2, and path 3 are 0.48 eV, 0.67 eV, and 0.35 eV, respectively. Remarkably, the path 3 is more favorable for Li migration on the surface of *Pmma*-CrP_2.

Finally, we will investigate the open-circuit-voltage (OCV) of the two predicted CrP_2 monolayers. As shown in Fig. 6, the OCV of CrP_2 monolayer at different Li concentration is calculated by employing the $2 \times 1 \times 1$ supercell. We note that OCV of *Pmmn*-CrP_2 monolayer decreases monotonously with the increasing Li concentration. Additionally, the values of OCV are in the range from 1.07 eV to 0.47 eV, which can prevent dendrites formation of Li metals during the charge/discharge process. Instead, the OCV of *Pmma*-CrP_2 is obviously fluctuant with the increase of Li concentration, indicating the instability of charge/discharge process. Based on these results, the more stable intercalation voltage renders *Pmmn*-CrP_2 monolayer a promising candidate for LIBs.

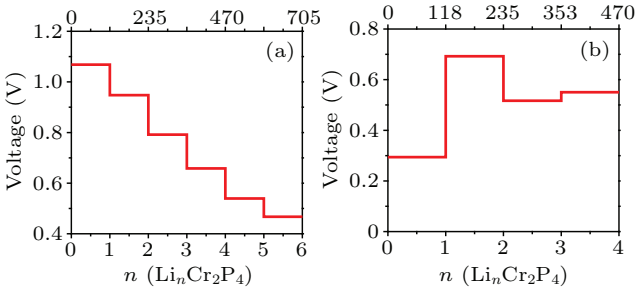


Fig. 6. The open circuit voltage profiles of Li on (a) *Pmmn*-CrP_2 and (b) *Pmma*-CrP_2.

4. Conclusions

In summary, we systematically studied electrode properties of two new monolayers *Pmmn*-CrP_2 and *Pmma*-CrP_2. The high mechanical, thermodynamics, and dynamic stability can increase the number of cycle life. In addition, the two monolayers possess a favorable Li storage capacity for LIBs. Especially, the specific capacity of *Pmmn*-CrP_2 reaches up to 705 $mA{\cdot}h{\cdot}g^{-1}$, originating from its unique atomic arrangements. Furthermore, the migration barrier of Li on the surfaces of *Pmmn*-CrP_2 is very low, which is beneficial to the charge/discharge rate. These above results show that *Pmmn*-CrP_2 monolayers could be quite promising 2D anode materials for LIBs. Our studies may motivate both experimental and theoretical efforts to further explore high-performance anode materials for ion battery.

Acknowledgements

Project supported by the National Natural Science Foundation of China (Grant No. 11964006), the Science and Technology Foundation of Kaili University (Grant No. 2022ZD06), and the Specialized Research Fund for the Doctoral Program of Kaili University (Grant Nos. BS201601 and BS201702).

References

[1] Qian J, Wu X, Cao Y, Ai X and Yang H 2013 *Angew. Chem. Int. Ed.* **52** 4633
[2] Zhang Y, Wang P, Zheng T, Li D, Li G and Yue Y 2018 *Nano Energy* **49** 596
[3] Chen S, Chen Z, Xu X, Cao C, Xia M and Luo Y 2018 *Small* **14** 1703361
[4] Jiang Y, Song D, Wu J, Wang Z, Huang S, Xu Y, Chen Z, Zhao B and Zhang J 2019 *ACS Nano* **13** 9100
[5] Chen F, Lin J, Chen Y, Dong B, Yin C, Tian S, Sun D, Xie J, Zhang Z, Li Hong and Li C 2022 *Chin. Phys. B* **31** 096301
[6] Yang J, Zou J, Luo C, Ran Q, Wang X, Chen P, Hu C, Niu X, Ji H and Wang L. 2021 *Chin. Phys. Lett.* **38** 068201
[7] Liu J, Liu C S, Ye X J and Yan X H 2018 *J. Mater. Chem. A* **6** 3634
[8] Shen Y, Liu J, Li X and Wang Q 2019 *ACS Appl. Mater. Interfaces* **11** 35661
[9] Bo T, Liu P F, Xu J, Zhang J, Chen Y, Eriksson O, Wang F and Wang B T 2018 *Phys. Chem. Chem. Phys.* **20** 22168
[10] Liang Y, Lai W H, Miao Z and Chou S L 2018 *Small* **14** 1702514
[11] Francis C F, Kyratzis I L and Best A S 2020 *Adv. Mater.* **32** 1904205
[12] Shi S, Gao J, Liu Y, Zhao Y, Wu Q, Ju W, Ouyang C and Xiao R 2016 *Chin. Phys. B* **25** 018212
[13] Wang Z, Wang D, Zou Z, Song T, Ni D, Li Z, Shao X, Yin W, Wang Y, Luo W, Wu M, Avdeev M, Xu B, Shi S, Ouyang C and Chen L 2020 *Nat. Sci. Rev.* **7** 1768
[14] Zhu C, Qu X, Zhang M, Wang J, Li Q, Geng Y Y, Ma Y and Su Z P 2019 *J. Mater. Chem. A* **7** 13356
[15] Zhao Z, Yu T, Zhang S, Xu H, Yang G and Liu Y 2019 *J. Mater. Chem. A* **7** 405
[16] Khan K, Tareen A K, Aslam M, Wang R, Zhang Y, Mahmood A, Ouyang Z, Zhang H and Guo Z 2020 *J. Mater. Chem. C* **8** 387
[17] Rao F Y, Ning F H, Jiang L W, Zeng X M, Wu M S, Xu B and Ouyang C Y 2016 *Chin. Phys. B* **25** 028202
[18] Wan M, Zhang Z, Zhao S and Zhou N 2022 *Chin. Phys. B* **31** 096301
[19] Ghosh A, Pal S and Sarkar P 2022 *J. Phys. Chem. C* **126** 5092
[20] Lv X, Wei W, Sun Q, Yu L, Huang B and Dai Y 2017 *ChemPhysChem* **18** 1627
[21] Pang J, Mendes R G, Bachmatiuk A, Zhao L Ta H Q, Gemming T, Liu H, Liu Z and Rummeli M H 2019 *Chem. Soc. Rev.* **48** 72
[22] Naguib M, Come J, Dyatkin B, Presser V, Taberna P L, Simon P, Michel W B and Gogotsi Y 2012 *Electrochem. Commun.* **16** 61
[23] Sun Q, Dai Y, Ma Y, Jing T, Wei W and Huang B 2016 *J. Phys. Chem. Lett.* **7** 937
[24] Yu Y. Guo Z, Peng Q, Zhou J and Sun Z 2019 *J. Mater. Chem. A* **7** 12145
[25] Tang Q, Zhou Z and Shen P 2012 *J. Am. Chem. Soc.* **134** 16909
[26] Anasori B, Lukatskaya M R and Gogotsi Y 2017 *Nat. Rev. Mater.* **2** 16098
[27] Xie Y, Naguib M, Mochalin V N, Barsoum M W, Gogotsi Y, Yu X, Nam K W, Yang X Q, Kolesnikov A I and Kent P R 2014 *J. Am. Chem. Soc.* **136** 6385
[28] Yu T, Zhang S, Li F, Zhao Z, Liu L, Xu H and Yang G. 2017 *J. Mater. Chem. A* **5** 18698
[29] Hu J, Wang Z, Zhang G, Liu Y, Liu N, Li W, Li J, Ouyang C and Yang S 2021 *Chin. Phys. B* **30** 046302
[30] Xu J, Wang D, Lian R, Gao X, Liu Y, Yury G and Wei Y 2019 *J. Mater. Chem. A* **7** 8873
[31] Huang H, Wu H H, Chi C, Huang B and Zhang T Y 2019 *J. Mater. Chem. A* **7** 8897
[32] Xu J, Wang D, Liu Y, Lian R, Gao X, Chen G and Wei Y 2019 *J. Mater. Chem. A* **7** 26858
[33] Yu T, Zhao Z, Liu L, Zhang S, Xu H and Yang G 2018 *J. Am. Chem. Soc.* **140** 5962
[34] Zhu C, Qu X, Zhang M, Wang J, Li Q, Geng Y, Ma Y and Su Z 2019 *J. Mater. Chem. A* **7** 13356
[35] Mayo M, Griffith K J, Pickard C J and Morris A J 2016 *Chem. Mater.* **28** 2011
[36] Zhao Z, Yu T, Zhang S, Xu H, Yang G and Liu Y 2019 *J. Mater. Chem. A* **7** 405
[37] Zhu J and Schwingenschlögl U P 2017 *2D Mater.* **4** 025073
[38] Wang Y, Lv J, Zhu L and Ma Y 2012 *Comput. Phys. Commun.* **183** 2063
[39] Kresse G and Hafner J 1993 *Phys. Rev. B* **47** 558
[40] Blöchl P E 1994 *Phys. Rev. B* **50** 17953
[41] Perdew J P, Burke K and Ernzerhof M 1996 *Phys. Rev. Lett.* **77** 3865
[42] Ming W, Yoon M, Du M H, Lee K and Kim S W. 2016 *J. Am. Chem. Soc.* **138** 15336
[43] Jing T, Liang D, Hao J, Deng M and Cai S 2019 *J. Chem. Phys.* **151** 024702
[44] Du A, Sanvito S and Smith S C 2012 *Phys. Rev. Lett.* **108** 197207
[45] Zhang Y, Wu Z F, Gao P F, Fang D Q, Zhang E H and Zhang S L 2017 *Phys. Chem. Chem. Phys.* **19** 2245
[46] Liu C S, Yang X L, Liu J and Ye X J 2018 *ACS Appl. Energy Mater.* **1** 3850
[47] Jing Y, Ma Y, Li Y and Heine T 2017 *Nano Lett.* **17** 1833
[48] Liu B, Gao T, Liao P, Wen Y, Yao M, Shi S and Zhang W 2021 *Phys. Chem. Chem. Phys.* **23** 18784
[49] Kudin K N, Scuseria G E and Yakobson B I 2001 *Phys. Rev. B* **64** 235406
[50] King A, Johnson G, Engelberg D, Ludwig W and Marrow J 2008 *Science* **321** 382
[51] Erickson E M, Ghanty C and Aurbach D 2014 *J. Phys. Chem. Lett.* **5** 3313
[52] Zhang T, Ma Y, Huang B and Dai Y 2019 *ACS Appl. Mater. Interfaces* **11** 6104
[53] Lv X, Wei W, Huang B and Dai Y 2019 *J. Mater. Chem. A* **7** 2165